RSC Advances

PAPER

View Article Online
View Journal | View Issue

Cite this: *RSC Adv.*, 2022, **12**, 10097

A study on the viscosity reduction mechanism of high-filled silicone potting adhesive by the formation of Al_2O_3 clusters

Jing Wang, Haihong Ma, Fengmei Ren, Zhengfa Zhou * and Weibing Xu

Heat dissipation has become a key problem for highly integrated and miniaturized electronic components. High thermal conductivity, good flowability and low coefficient of linear thermal expansion (CLTE) are indispensable performance parameters in the field of electronic potting composite materials. In this study, spherical alumina (Al_2O_3) was surface modified by γ-(2,3-epoxypropoxy) propyltrimethoxy silane (KH560) and γ-aminopropyltriethoxy silane (KH550) and labelled as Al_2O_3-epoxy and Al_2O_3–NH_2, respectively. Al_2O_3-epoxy and Al_2O_3–NH_2 powders were equally filled in vinyl silicone oil to prepare a high Al_2O_3 loading (89 wt%) precursor of silicone potting adhesive. The viscosity of the precursor rapidly decreased with increasing reaction time of Al_2O_3-epoxy and Al_2O_3–NH_2 at 140 °C. The viscosity reduction mechanism may be due to the formation of some Al_2O_3 clusters by the reaction of Al_2O_3-epoxy with Al_2O_3–NH_2, which results in some vinyl silicone oil segments being held in the channel of particles through capillary phenomenon, leading to the friction among Al_2O_3 clusters decreasing considerably. Laser particle size analysis and scanning electron microscopy (SEM) results confirmed the existence of Al_2O_3 clusters. Energy dispersive spectroscopy (EDS) and dynamic viscoelasticity experiments revealed that some segments of vinyl silicone oils were held by Al_2O_3 clusters. When Al_2O_3-epoxy and Al_2O_3–NH_2 reacted for 4 h, the thermal conductivity, CLTE and volume electrical resistivity of the silicone potting adhesive reached 2.73 W m^{-1} k^{-1}, 75.8 ppm/°C and 4.6 × 10^{13} Ω cm, respectively. A new strategy for preparing electronic potting materials with high thermal conductivity, good flowability and low CLTE is presented.

Received 29th December 2021
Accepted 15th March 2022

DOI: 10.1039/d1ra09417c

rsc.li/rsc-advances

1. Introduction

The potting operation of electronic devices can not only improve the dust-proof, moisture-proof and anti-vibration performance of devices, but also be conducive to the miniaturization and lightweight of devices.[1] Electronic potting materials usually include epoxy resin (EP), polyurethane, and silicone. Epoxy resin potting adhesive has high hardness, good adhesion, and low CLTE (50–70 ppm/°C),[2] while the repairability of the device is poor.[3,4] Polyurethane potting adhesive has good elasticity and anti-vibration performance, but its thermal resistance is poor (usually lower than 150 °C).[5] Silicone has good elasticity, wide working temperature range of minus 60 to 200 °C, and excellent repairability of the device.[6–8] As a result, silicone potting adhesive is now used in many electronic devices.

In recent years, electronic devices are developing towards high integration and miniaturization. The heat generated by devices needs to be diffused in time to improve the operation reliability and service life of devices.[9,10] The thermal conductivity of silicone is low (~0.2 W m^{-1} k^{-1}),[11,12] which cannot meet the working requirements of potting materials. Thermally conductive but insulating fillers such as boron nitride (BN),[13,14] Al_2O_3,[15] aluminum nitride (AlN),[16] and silicon carbide (SiC)[17] are often filled to improve the thermal conductivity of silicone potting adhesive. However, the thermal conductivity of polymer-based composites with fillers is relatively low. Preparation of 3D fillers, filler assembling and orientation can effectively improve the thermal conductivity of polymer composites.[18–21] Li *et al.*[22] used the ice template method to assemble BN nanosheets (BNNSs) and silver nanowires (AgNWs), and the thermal conductivity of the composites reached 1.10 W m^{-1} k^{-1} when the filler addition was only 5.0 vol%. Yang *et al.*[23] prepared a thermally conductive filler with BN bridging carbon fiber (CF), and a special three-dimensional oriented BN/CF/EP composite material was obtained by the vacuum impregnation method, improving the thermal conductivity to 3.1 W m^{-1} k^{-1}. Song *et al.*[24] prepared 3D-Al_2O_3/silicone rubber (SR) frame by a foaming and vacuum infiltration process, and the thermal conductivity of the composite reached 0.747 W m^{-1} k^{-1} when the loading amount of Al_2O_3 was 32.6 wt%. Liu *et al.*[25] obtained 35 wt% BN/30 wt%

School of Chemistry and Chemical Engineering, Hefei University of Technology, Hefei, 230009, People's Republic of China. E-mail: zhengfazhou@hfut.edu.cn; Tel: +86-551-62901455

Al_2O_3/polydimethylsiloxane (PDMS) composite materials through a 3-D printing assisted orientation technology, in which the orientation rate and thermal conductivity reached 90.65% and 3.64 W m^{-1} k^{-1}, respectively. The CLTE of silicone is usually higher than 200 ppm/°C.[26] Although 3D fillers, filler orientation and self-assembling can improve the thermal conductivity of silicone composites to a certain extent, the CLTE of these composites are often too large to satisfy the potting requirements of specific electronic devices. Thermally conductive but insulating fillers such as Al_2O_3 have low CLTE (~6.6 ppm/°C),[27] which can meet the performance requirements of high thermal conductivity and low CLTE of silicone potting adhesive under the condition of large amount of filling. For example, Fu *et al.*[28] prepared a series of dense boric acid modified BNNSs/EP composites by mechanical ball milling and pressure forming processes; the EP composites with 90 wt% BNNSs achieved the maximum thermal conductivity (6.7 W m^{-1} k^{-1}) and the minimum CLTE (4.5 ppm/°C) at a temperature of 25 °C. Unfortunately, high filler loading will inevitably cause a sharp increase in the viscosity of silicone potting adhesive, which makes it impossible to achieve potting under mechanical or artificial conditions.[29]

In this study, Al_2O_3-epoxy and Al_2O_3–NH_2 powders were equally filled in vinyl silicone oil to prepare a high Al_2O_3 loading (89 wt%) precursor of silicone potting adhesive. The viscosity of the precursor was greatly reduced through the reaction of Al_2O_3-epoxy and Al_2O_3–NH_2 powders, and a mechanism of viscosity reduction was proposed. The experimental results of laser particle size analysis, SEM, EDS, and dynamic viscoelasticity analysis supported the proposed viscosity reducing mechanism. This study presents a new strategy for preparing electronic potting materials with high thermal conductivity, low viscosity and low CLTE.

2. Experimental

2.1. Materials

Vinyl silicone oil (50 cp) and hydrogen-containing silicone oil (H = 0.8 wt%) were provided by Jiande City Sifco Materials Co., Ltd. (China). Spherical alumina (AX10-32, Al_2O_3) with a mean particle size of 8.7 μm was supplied by Nippon Steel Corporation (Japan). γ-Aminopropyltriethoxy silane (KH550) and γ-(2,3-epoxypropoxy) propyltrimethoxy silane (KH560) were purchased from Changzhou Runxiang Chemical Co., Ltd (China) with a purity of 99%. Platinum catalysts (1000 ppm) were obtained from Shanghai Guiyou New Materials Technology Ltd. (China). Absolute ethanol, toluene and tetrahydrofuran (THF) were purchased from Aladdin Industrial Corporation (China). All reagents were used as received without any further purification except vinyl silicone oil.

2.2. Surface treatment of Al_2O_3

Al_2O_3 powders were modified by 1 wt% KH550 and KH560, respectively. The treatment process was the same as in our previous paper.[30] 8 g KH550 was mixed with water and ethanol (the molar ratio of KH550 to water was 1 : 3, the volume ratio of KH550 to ethanol was 1 : 1) and hydrolyzed at 30 °C for 30 min to prepare KH550 hydrolysate. 800 g Al_2O_3 powders were added into the high-speed mixer (SHR-10A, Zhangjiagang Beier Machinery Co., Ltd. China). When the temperature of Al_2O_3 powders in the high-speed mixer reached 110 °C, KH550 hydrolysate was sprayed and stirred at 1000 rpm for 25 min. The KH550 treated Al_2O_3 was washed three times using absolute ethanol to remove the ungrafted KH550, and dried in a vacuum oven at 105 °C for 5 h. The preparation of KH560 modified Al_2O_3 was the same as above.

2.3. Preparation of precursor

The vinyl silicone oil was vacuum dried at 125 °C for 3 h to remove volatile matter before using. The mass ratio of Al_2O_3-epoxy and Al_2O_3–NH_2 was set as 1 : 1, and the amount of Al_2O_3 in the mixture of surface-treated Al_2O_3 and vinyl silicone oil was set as 89 wt%. The mixing process was carried out in a high-speed disperser (JFS-1100A, Laizhou Wankai Machinery Co., Ltd. China) at 2000 rpm for 20 min at 30 °C using cooling water, then the mixture was transferred to a three-necked flask with a mechanical stirrer at 600 rpm in an oil bath and reacted at 140 °C for 0.5 h, 1 h, 2 h, 3 h, and 4 h, respectively, to prepare the precursor of silicone potting adhesive. The epoxy and amino groups on the surface of Al_2O_3 can react to different degrees. The mixture directly coming from the high-speed disperser was indicated as the precursor of 0 h reaction time for comparison.

2.4. Preparation of silicone potting adhesive

1000 g precursor was mixed with 1 g platinum catalysts and 2.0 g hydrogen-containing silicone oil, respectively, to prepare the A and B components of silicone potting adhesive.

2.5. Characterization

X-ray photoelectron spectroscopy (XPS) was utilized to measure elemental content on the surface of Al_2O_3 powders by ESCALAB 250Xi (Thermo Electron Corporation, USA).

Thermogravimetric analysis (TG) was carried out on a TGA8000 analyzer (PerkinElmer, USA) at a heating rate of 10 °C min^{-1} under a nitrogen atmosphere from 25 °C to 700 °C.

Shear viscosity was obtained using the NDJ-97 type rotary viscometer (Shanghai Changji, China) at 25 °C. The experiment was repeated three times.

Mastersizer 2000 laser particle size analyzer (Malvern Instruments, UK) was used to detect the particle size distribution. 10 g precursor was added in 100 mL toluene under stirring for 10 min, and allowed to settle naturally; the sediments were then collected. This operation was repeated three times to obtain particle sediments. The particle sediments were dispersed in absolute ethanol for testing, and the concentration of the sediments was 0.09%.

Dynamic viscoelasticity analysis of the precursor was performed using small amplitude oscillatory shear (SAOS) at 25 °C, on a Malvern Rheometer (HRnano 200, UK) equipped with cone-and-plate fixture. The diameter of the cone-and-plate was 20 mm, the inclination angle was 2°, and the fixed strain was 1%. Pre-shearing was performed before each dynamic

viscoelasticity experiment to eliminate the shear history of the samples.

Gemini 500 field emission scanning electron microscope (Carl Zeiss, German) was utilized to observe the morphology of Al_2O_3 clusters. The washing operation of the precursor was the same as the laser particle size analysis, where the sediments were fully dispersed in 50 mL THF, then a drop was taken and dripped on the copper mesh, and dried at 80 °C for 2 h. Before testing, the samples were treated with gold spraying. The distribution of elements was obtained by a high-resolution field emission scanning electron microscope equipped with energy dispersive spectroscopy (Regulus 8230, Japan), and testing pattern was selected to use high-end plane insertion energy spectrum, to eliminate shooting shadow.

TPS 2500S thermal analyzer (Hot Disk, Sweden) was used to characterize the thermal conductivity of silicone potting composite materials, in which the double helix probe of 4 mm diameter was sandwiched between two lamella samples of 2 mm thickness. The CLTE was measured on a TMA402F3 thermo-mechanical analyzer (NETZSCH, German) from 25 °C to 250 °C at a heating rate of 10 °C min^{-1}. ZST-121 volume surface resistivity tester (Beijing Zhonghang Times Instrument Equipment, China) was utilized to determine the volume resistivity, and the diameter and thickness of the sample was 8 mm and 2 mm, respectively. The components A and B of silicone potting adhesive were mixed under equal mass. After complete stirring, the mixture was injected into the mold, and vacuumed to eliminate air bubbles. The mixture was cured at 90 °C for 3 h, and then demolded to obtain thermal and insulating test samples.

3. Results and discussion

3.1. Surface treatment of Al_2O_3 powders

Fig. 1 shows the XPS spectra of Al_2O_3-epoxy, Al_2O_3–NH_2, and pristine Al_2O_3 powders, and the content of Si 2p, C 1s, N 1s, and O 1s are provided in Table 1. The C and Si atom content of

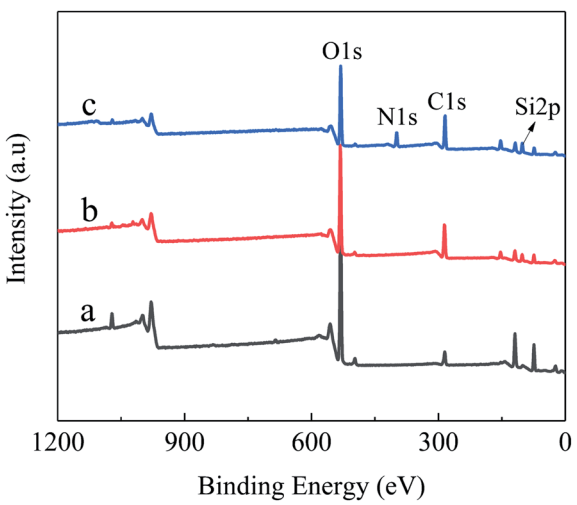

Fig. 1 XPS spectra of powders (a) Pristine Al_2O_3, (b) Al_2O_3-epoxy, (c) Al_2O_3–NH_2.

Table 1 Element composition on the surface of powders

Sample	Si 2p (%)	C 1s (%)	N 1s (%)	O 1s (%)
Pristine Al_2O_3	1.85	17.70	0.80	79.65
Al_2O_3-epoxy	8.08	42.64	0	49.28
Al_2O_3–NH_2	11.46	40.08	10.50	37.96

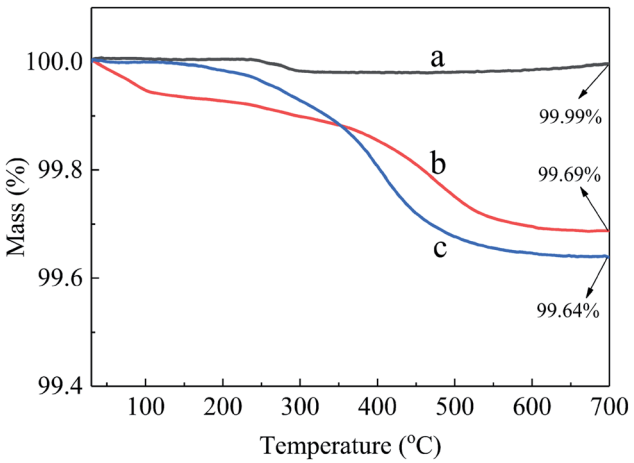

Fig. 2 TG curves of powders (a) pristine Al_2O_3, (b) Al_2O_3-epoxy, (c) Al_2O_3–NH_2.

Al_2O_3-epoxy and Al_2O_3–NH_2 was higher than that of pristine Al_2O_3 powders, while the oxygen element content of Al_2O_3-epoxy and Al_2O_3–NH_2 was lower than that of pristine Al_2O_3. The N element content of Al_2O_3–NH_2 was considerably higher than that of pristine Al_2O_3. The results show that KH560 and KH550 are successfully grafted onto the surface of Al_2O_3 powders, respectively.[31]

Fig. 2 shows the TG curves of pristine and modified Al_2O_3. The mass retention rate (at 700 °C) of pristine Al_2O_3, Al_2O_3-epoxy, Al_2O_3–NH_2 was 99.99%, 99.69%, and 99.64%, respectively. The mass loss of pristine Al_2O_3 came from the decomposition of the surface free hydroxyl group at high temperature, whereas the weight loss of Al_2O_3-epoxy and Al_2O_3–NH_2 came from the decomposition of not only the free hydroxyl group but also the organic residues of KH560 or KH550 on the surface of Al_2O_3-epoxy and Al_2O_3–NH_2 powders. The amount of residual silane agent grafted on the surface of inorganic powders can be obtained by comparing the mass retention rate difference between pristine and modified inorganic powders.[32] A drop in the thermogram of Al_2O_3-epoxy at 100 °C (0.05%) might be coming from extraneous water, which should be eliminated while calculating the amount of residual KH560 grafted on the surface of Al_2O_3-epoxy. As a result, the amount of residual KH560 and KH550 grafted on the surface of Al_2O_3-epoxy and Al_2O_3–NH_2 was 0.25% and 0.35%, respectively.

3.2. Effect of reaction time on viscosity

The viscosity of potting adhesive has a great impact on the stable production and performance consistency of electronic devices.[33] Fig. 3 shows the effect of reaction time of Al_2O_3-epoxy

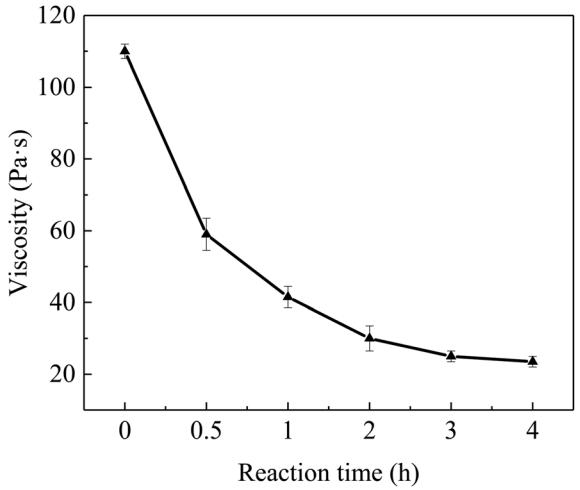

Fig. 3 The viscosity of the mixture *versus* Al_2O_3-epoxy and Al_2O_3–NH_2 reaction time.

and Al_2O_3–NH_2 at 140 °C on the viscosity of the mixture of vinyl silicone oil filled with surface modified Al_2O_3. The Al_2O_3 loading amount was 89 wt%, and the viscosity of the mixture decreased significantly with increasing reaction time. The viscosity reached 110 Pa s when the reaction time was 0 h, and the mixture had difficulty to flow in this state. After Al_2O_3-epoxy and Al_2O_3–NH_2 reacted for 0.5 h, the viscosity of the mixture had dropped about 46.4% of the initial viscosity. The viscosity dropped by 78.6% to 23.5 Pa s when the reaction time was 4 h, and the mixture flowed easily at this point.

It is well known that Richard summarized the effect of particle interaction coefficient (σ) on the viscosity of the particle filling system.[34] When $\sigma = 0$, the suspension viscosity equation was simplified as $\ln(\eta/\eta_0) = [\eta]\varphi$, where η is suspension viscosity, η_0 and $[\eta]$ are viscosity and intrinsic viscosity of suspending medium, respectively, and φ is suspension particle volume fraction. For the case $\sigma = 2$, the suspension viscosity equation is $\ln(\eta/\eta_0) = [\eta]\{\varphi/(1 - \varphi/\varphi_n)\}$, where, φ_n is the maximum particle packing fraction. He concluded that the viscosity of the particle filling mixture increased rapidly with increasing σ. In this work, the φ of Al_2O_3 was 0.68. Assuming φ_n was 0.95, when the σ increased from 0 to 2, η would increase $e^{1.71[\eta]}$ times by the above formula. However, the experimental results showed that the viscosity in this work decreased significantly with increasing particle interaction. This abnormal phenomenon may be due to the micro aggregation of Al_2O_3 particles, which will be discussed later.

3.3. Viscosity reduction mechanism

The epoxy groups of Al_2O_3-epoxy can react with the amino groups of Al_2O_3–NH_2 in vinyl silicone oil, resulting in the formation of micro aggregation of Al_2O_3 particles as shown in Fig. 4(a). The chemical bond coming from the reaction of the epoxy and amino groups makes Al_2O_3 particles contact closely. As a result, tiny pore channels are generated and some vinyl silicone oil segments might immerse in the channels due to capillary phenomenon (Fig. 4(b)). The fixed vinyl silicone oil acts as a lubricator and significantly reduces the friction among Al_2O_3 clusters, so the viscosity of the Al_2O_3-epoxy and Al_2O_3–NH_2 reaction system was considerably lower than that of the non-reacting system.

3.4. Experimental results supporting the viscosity reduction mechanism

Fig. 5 shows the effect of reaction time of Al_2O_3-epoxy and Al_2O_3–NH_2 at 140 °C on the particle size and particle size distribution of Al_2O_3, and the corresponding data is shown in

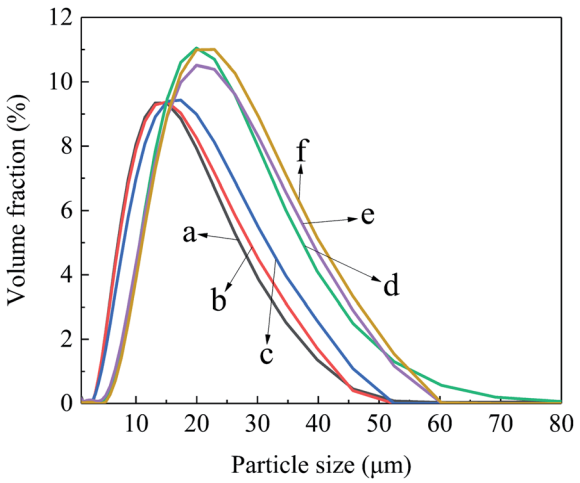

Fig. 5 The particle size distribution curves of Al_2O_3 with different reaction time (a) 0 h, (b) 0.5 h, (c) 1 h, (d) 2 h, (e) 3 h, (f) 4 h.

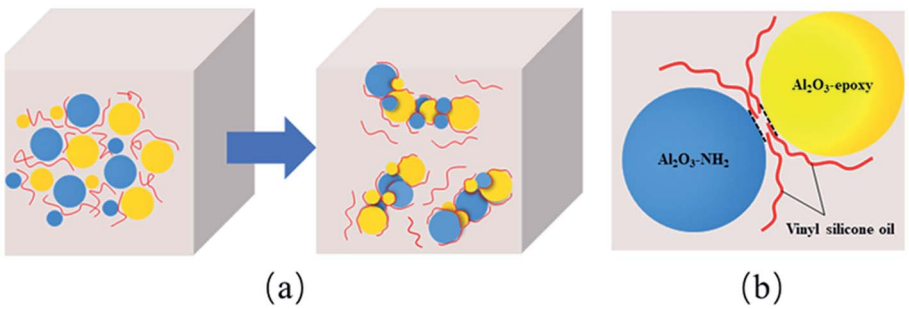

Fig. 4 Diagrams of (a) formation of Al_2O_3 clusters, (b) some vinyl silicone oil segments fixing in the interval of particles.

Table 2 The D_{10}, D_{50} and D_{90} of Fig. 5

Reaction time/h	D_{10}/μm	D_{50}/μm	D_{90}/μm
0	5.79	12.55	25.21
0.5	6.18	13.07	26.10
1	6.67	14.39	28.31
2	9.53	18.36	33.85
3	8.97	18.35	33.69
4	10.11	19.30	34.71

Table 2. The D_{10}, D_{50} and D_{90} increased significantly with prolonged reaction time. There was a jump in particle size distribution between 1 h and 2 h reaction times. This phenomenon may be because the degree of epoxy group reacting with the amino group is considerably low at 1 h, but gets much higher at 2 h. The SEM images (Fig. 6) also show that the size of Al_2O_3 clusters at 2 h is considerably larger than that at 1 h.

Fig. 6 shows the SEM images of Al_2O_3 with Al_2O_3-epoxy and Al_2O_3–NH_2 reacting for different reaction times at 140 °C. It can be seen that the particle distribution was relatively loose when the reaction time was 0 h (Fig. 6(a)). When epoxy groups reacted with amino for 0.5 h to 1 h, the modified Al_2O_3 particles showed slight aggregation and the size of the Al_2O_3 clusters was small (Fig. 6(c)). The Al_2O_3 clusters became larger at 2 h reaction time, which was consistent with the results of particle size distribution shown in Fig. 5, and the Al_2O_3 particles were in close contact with each other (Fig. 6(d)). The size of Al_2O_3 clusters was getting larger and larger when the reaction time exceeded 3 h (Fig. 6(e and f)).

Fig. 7 shows the visual element distribution observed by EDS of Al_2O_3 with Al_2O_3-epoxy and Al_2O_3–NH_2 reacting for different reaction times. From Fig. 7(a), when the reaction time was 0 h, the images of Al and O elements revealed that the Al_2O_3 particles were discrete from each other, and the image of Si element was unclear. Fig. 7(b) and (c) display the Al, O and Si images of Al_2O_3 with Al_2O_3-epoxy and Al_2O_3–NH_2 reacting for 1 h and 4 h, respectively. It was found that some Al_2O_3 particles contacted tightly, and some Si elements appeared on the surface and interval of Al_2O_3 particles. Furthermore, the Si element in Fig. 7(c) was higher and more significant than that in Fig. 7(b) as

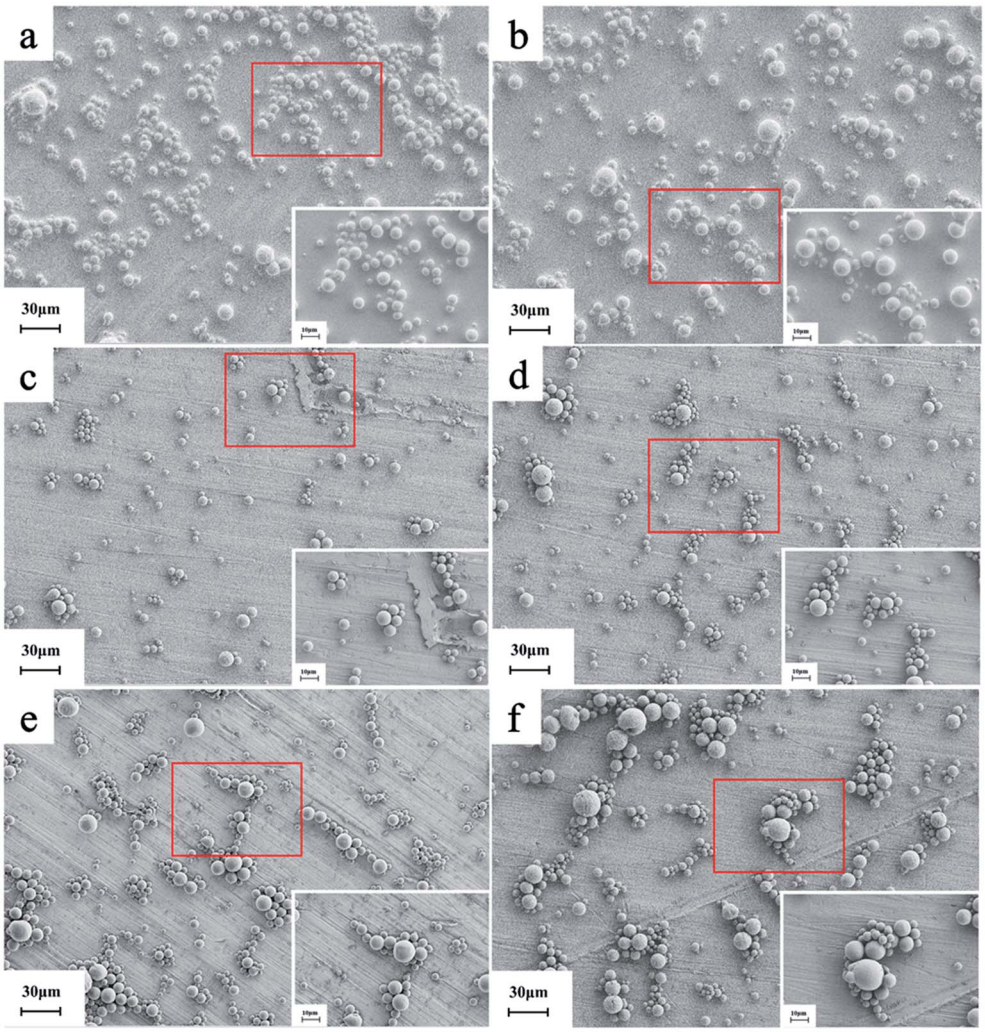

Fig. 6 The SEM images of Al_2O_3 with different reaction time (a) 0 h, (b) 0.5 h, (c) 1 h, (d) 2 h, (e) 3 h, (f) 4 h.

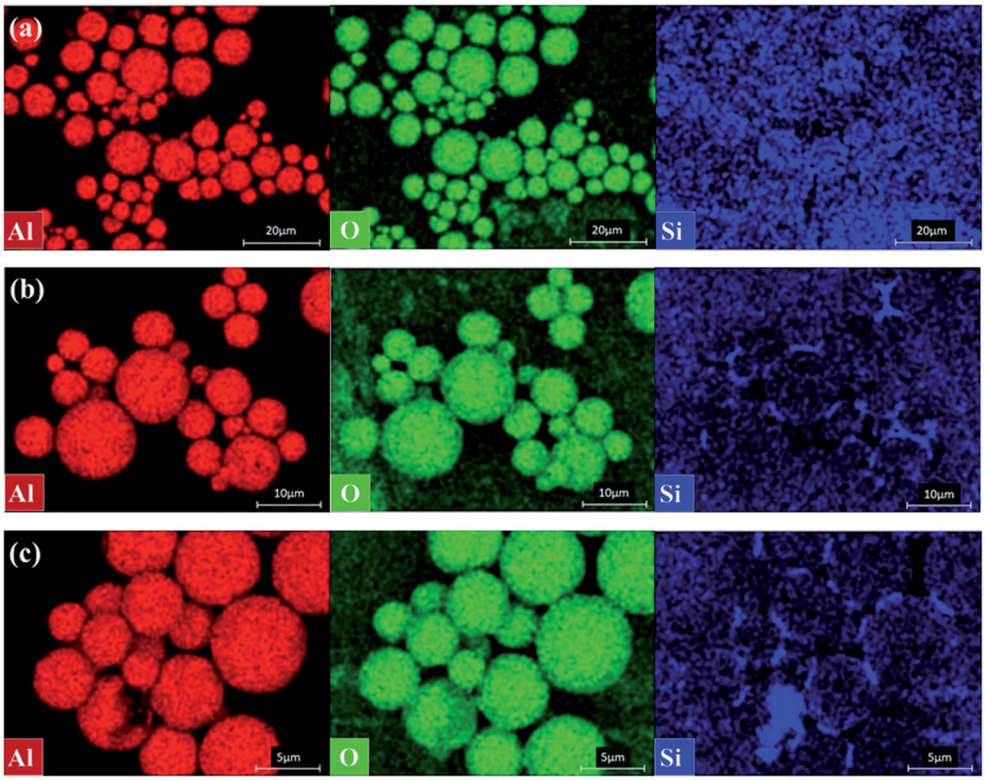

Fig. 7 The Al, O and Si element images of Al_2O_3 with different reaction time (a) 0 h, (b) 1 h, (c) 4 h.

the reaction time of Al_2O_3-epoxy and Al_2O_3–NH_2 was prolonged. This phenomenon indicates that some vinyl silicone oil segments are fixed in the intervals of Al_2O_3 particles as described in Fig. 4(b).

Fig. 8 shows the dynamic viscoelasticity curves of precursors in which Al_2O_3-epoxy reacts with Al_2O_3–NH_2 for different reaction times. Fig. 8(a) shows the curve of the complex viscosity η^* *versus* angular frequency ω. When the reaction time was 0 h, the precursor exhibited significantly low-frequency shear thinning,[35] while the precursor with powders reacting for 4 h exhibited weak shear thinning at low frequency, and both samples showed shear thickening behavior at high frequency. The change in viscosity is related to a certain structural change inside the liquid. Giuntoli *et al.*[36] studied the α relaxation kinetic model of a coarse-grained polymer melt under steady-state shear. They found that the shear thinning was due to the action of shearing, the instantaneous combination of macromolecules was "deaggregated" or the fixed particle clusters were destroyed. In this study, when the epoxy and amino groups grafted on the Al_2O_3 surface did not undergo a chemical reaction, the Al_2O_3 powders were evenly dispersed in the vinyl silicone oil. Only electrostatic interaction, van der Waals forces and solvation exist among modified Al_2O_3 powders, and between powders and vinyl silicone oil. Under shear force, the electrostatic attraction, van der Waals forces and solvation were destroyed, and at this moment, the chain of vinyl silicone oil was untangled, resulting in remarkable shear thinning. On the contrary, when the two groups reacted, a chemical bonding interaction was generated among Al_2O_3 powders to form Al_2O_3 clusters. A part of the vinyl silicone oil was fixed in the tiny intervals due to capillary phenomenon, which has a lubricating effect resulting in reduced interaction among the Al_2O_3 clusters. Hence, the shear thinning phenomenon was weakened.

Fig. 8 (b) and (c) are the curves of the elastic modulus (G') and viscous modulus (G'') *versus* the angular frequency ω of precursor with the reaction time of 0 h and 4 h, respectively. It could be clearly seen from the figure that when ω was low, the G' and G'' of the precursor were basically the same at 0 h reaction time. Whereas the G'' was higher than G' when the reaction time was 4 h. It was because that Al_2O_3-epoxy and Al_2O_3–NH_2 took reaction to build a Al_2O_3 cluster structure as shown in Fig. 6. Some segments of vinyl silicone oil were fixed in the particle intervals, which deeply limited the movement ability of the vinyl silicone oil, resulting in its prolonged relaxation time. The relationship between loss factor tan δ and ω in Fig. 8(d) further showed that the mechanical loss of the Al_2O_3-epoxy and Al_2O_3–NH_2 reacting system was higher than that of the non-reacting system at lower frequency. As the frequency increased, both G' and G'' showed an increasing trend, but the increasing speed of G′ exceeded that of G''. For the non-reacting system, the intersection of G' and G'' appeared at 99.58 rad s^{-1}, while for the 4 h reaction system, the intersection appeared at 39.64 rad s^{-1}, indicating that the elastic modulus of the 4 h reaction system is greatly improved. The results may be due to the formation of Al_2O_3 clusters in the 4 h reaction system, and Al_2O_3 clusters are of a bigger size, which increases the rigidity of the precursor at

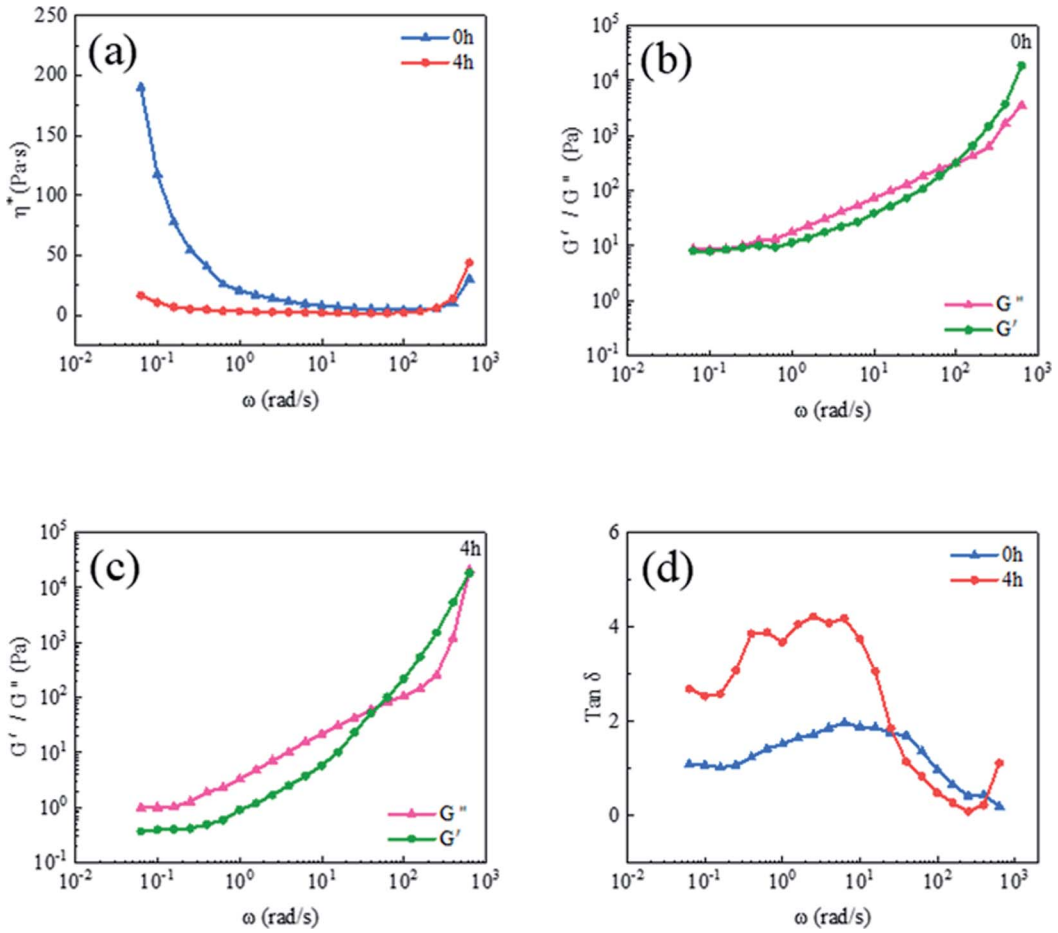

Fig. 8 The dynamic viscoelasticity curves of precursors with different reaction time, (a) η^* *versus* ω, (b) and (c) G' and G'' *versus* ω, and (d) tan δ *versus* ω.

Table 3 Thermal and insulating properties of silicone potting adhesive

Reaction time (h)	0	0.5	1	2	3	4
Thermal conductivity (W m^{-1} k^{-1})	2.67	2.69	2.70	2.67	2.71	2.73
CLTE (ppm/°C)	74.0	73.1	72.4	75.5	74.9	75.8
Volume electrical resistivity (X 10^{13} Ω cm)	5.7	4.8	2.5	6.4	7.3	4.6

higher frequency. Zheng *et al.*[37] found that higher G′ depended on larger size and the interaction between aggregations, which is conducive to flocculating a stable 3D network structure.

3.5. Thermal and insulating properties

The effect of reaction time of modified Al_2O_3 on the performance of silicone potting adhesive is shown in Table 3. The reaction time had little effect on the thermal conductivity, CLTE and the volume electrical resistivity of silicone potting adhesive. In the 4 h reaction system, the thermal conductivity, CLTE and volume electrical resistivity were 2.73 W m^{-1} k^{-1}, 75.8 ppm/°C and 4.6 × 10^{13} Ω cm, respectively. The viscosity of silicone potting adhesive for the 4 h reaction system was 19.2 Pa s, which satisfies the demands of a heat conduction insulation potting material.

4. Conclusions

This work found that the viscosity reduction of silicone potting adhesive was related to the formation of filler clusters. Al_2O_3-epoxy and Al_2O_3–NH_2 were successfully obtained by surface silanization. The viscosity of the precursor decreased significantly with an increase in the reaction time of Al_2O_3-epoxy and Al_2O_3–NH_2. The viscosity of the 4 h reaction system was only 78.6% of 0 h. The reason for this phenomenon might be that chemical bonding interaction among modified Al_2O_3 powders promoted the formation of Al_2O_3 clusters; some segments of vinyl silicone oils were fixed in tiny particle pore channels through capillary phenomenon, leading to a remarkable lubrication effect of Al_2O_3 clusters. Particle size distribution and SEM results revealed the formation of Al_2O_3 clusters. EDS

evidently showed the existence of vinyl silicone oil in the particle intervals of clusters. The dynamic viscoelasticity experimental results also supported the assumed viscosity reduction mechanism. Moreover, the as-prepared silicone potting adhesive possessed excellent thermal conductivity, low CLTE and low viscosity.

Author contributions

Jing Wang: methodology, validation, formal analysis, investigation, data curation, writing – original draft. Haihong Ma: investigation, validation, writing – review & editing. Fengmei Ren: investigation, validation. Zhengfa Zhou: methodology, investigation, validation, writing – review & editing. Weibing Xu: supervision, project administration, funding acquisition.

Conflicts of interest

There are no conflicts to declare.

Acknowledgements

The authors are grateful for the support and funding from Anhui Science and Technology Department, China (17030901076).

References

1 S. A. Meguid, C. Zhuo and F. Yang, *J. Electron. Packag.*, 2014, **136**, 041010.
2 T. Li, J. Zhang, H. P. Wang, Z. N. Hu and Y. F. Yu, *ACS Appl. Mater. Interfaces*, 2013, **5**, 8968–8981.
3 H. Chun, S. Y. Park, S. J. Park and Y. J. Kim, *Polymer*, 2020, **207**, 122916.
4 J. C. Foster, C. L. Staiger, J. W. Dugger and E. M. Redline, *ACS Macro Lett.*, 2017, **10**, 940–944.
5 N. H. Li, J. P. Liu, X. B. Liu, W. W. Yang, K. P. Song and X. L. Li, *IOP Conf. Ser.: Mater. Sci. Eng.*, 2020, **774**, 012089.
6 Y. Xue, X. F. Li, H. S. Wang, F. Zhao, D. H. Zhang and Y. F. Chen, *Mater. Des.*, 2019, **165**, 107580.
7 K. P. Ruan, H. Yan, S. J. Zhang, X. T. Shi, Y. Q. Guo and J. W. Gu, *Compos. Sci. Technol.*, 2021, **210**, 108799.
8 Y. G. Ouyang, X. F. Li, F. Ding, L. Y. Bai and F. L. Yuan, *Compos. Sci. Technol.*, 2020, **190**, 108019.
9 X. T. Yang, C. B. Liang, T. B. Ma, Y. Q. Guo, J. Kong, J. W. Gu, M. J. Chen and J. H. Zhu, *Adv. Compos. Hybrid Mater.*, 2018, **1**, 207–230.
10 M. Shtein, R. Nadiv, M. Buzaglo and O. Regev, *ACS Appl. Mater. Interfaces*, 2015, **7**, 23725–23730.
11 D. Yang, Q. G. Wei, B. Y. Li, L. Y. Yu, Y. F. Ni and L. Q. Zhang, *Composites, Part A*, 2021, **14**, 106260.
12 D. Liu, Q. Q. Kong, H. Jia, L. J. Xie, J. P. Chen, Z. C. Tao, Z. Wang, D. Jiang and C. M. Chen, *Carbon*, 2021, **18**, 216–224.
13 D. X. Liu, C. G. Ma, H. T. Chi, S. H. Li, P. Zhang and P. B. Dai, *RSC Adv.*, 2020, **10**, 42584–42595.
14 C. Y. Xu, M. Miao, X. F. Jiang and X. B. Wang, *Compos. Commun.*, 2018, **10**, 103–109.
15 Y. G. Ouyang, L. Y. Bai, H. F. Tian, X. F. Li and F. L. Yuan, *Composites, Part A*, 2022, **152**, 106685.
16 Z. L. Wei, W. Q. Xie, B. Z. Ge, Z. J. Zhang, W. L. Yang, H. Y. Xia, B. Wang, H. Y. Jin, N. K. Gao and Z. Q. Shi, *Compos. Sci. Technol.*, 2020, **199**, 108304.
17 Y. M. Yao, X. D. Zhu, X. L. Zeng, R. Sun, J. B. Xu and C. P. Wong, *ACS Appl. Mater. Interfaces*, 2018, **10**, 9669–9678.
18 H. Y. Chen, V. V. Ginzburg, J. Yang, Y. F. Yang, W. Liu, Y. Huang, L. B. Du and B. Chen, *Prog. Polym. Sci.*, 2016, **59**, 41–85.
19 F. Zhang, Y. Y. Feng and W. Feng, *Mater. Sci. Eng. R*, 2020, **142**, 100580.
20 X. M. Zhang, J. J. Zhang, L. C. Xia, C. H. Li, J. F. Wang, F. Xu, X. L. Zhang, H. Wu and S. Y. Guo, *ACS Appl. Mater. Interfaces*, 2017, **9**, 22977–22984.
21 Y. Hue, H. S. Wang, X. F. Li and Y. F. Chen, *Composites, Part A*, 2021, **144**, 106336.
22 H. T. Li, C. J. Fu, N. Chen, T. Zhang, J. M. Liu, G. P. Du, L. L. Ren, X. L. Zeng and R. Sun, *Compos. Commun.*, 2021, **25**, 100601.
23 Y. Wang, Y. Gao, B. Tang, X. F. Wu, J. Chen, L. M. Shan, K. Sun, Y. T. Zhao, K. Yang, J. H. Yu and W. G. Li, *RSC Adv.*, 2021, **11**, 25422–25430.
24 J. N. Song, L. Wu and Y. Zhang, *Polym. Bull.*, 2020, **77**, 2139–2153.
25 M. J. Liu, S. W. Chiang, X. D. Chu, J. Li, L. Gan, Y. B. He, B. H. Li, F. Y. Kang and H. D. Du, *Ceram. Int.*, 2020, **46**, 20810–20818.
26 N. Suzuki, S. Kiba, Y. Kamachi, N. Miyamoto and Y. Yamauchi, *J. Mater. Chem.*, 2011, **21**, 5338–5344.
27 Y. J. Wan, G. Li, Y. M. Yao, X. L. Zeng, P. L. Zhu and R. Sun, *Compos. Commun.*, 2020, **19**, 154–167.
28 K. Fu, J. W. Yang, C. C. Cao, Q. H. Zhai, W. Qiao, J. X. Qiao, H. J. Gao, Z. Zhou, J. W. Ji and M. Y. Li, *ACS Appl. Mater. Interfaces*, 2021, **13**, 2853–2867.
29 Y. Hu, C. Chen, Y. F. Wen, Z. G. Xue, X. P. Zhou, D. Shi, G. H. Hu and X. L. Xie, *Compos. Sci. Technol.*, 2021, **209**, 108760.
30 F. M. Ren, R. Zhou, F. Sun, H. H. Ma, Z. F. Zhou and W. B. Xu, *RSC Adv.*, 2017, **7**, 29779–29785.
31 Q. Guo, P. L. Zhu, G. Li, J. J. Wen, T. Y. Wang, D. Q. Lu, R. Sun and C. P. Wong, *Composites, Part B*, 2017, **116**, 388–397.
32 Y. M. Han, J. Y. Zhang, Q. Y. Yang, L. Shi, S. C. Qi and R. G. Jin, *J. Appl. Polym. Sci.*, 2008, **107**, 3788–3795.
33 C. Chen, Y. Xue, X. W. Li, Y. F. Wen, J. W. Liu, Z. G. Xue, D. A. Shi, X. P. Zhou, X. L. Xie and Y. W. Mai, *Composites, Part A*, 2019, **118**, 67–74.
34 R. D. Sudduth, *J. Appl. Polym.*, 1993, **48**, 37–55.
35 J. E. Butler and B. Snook, *Annu. Rev. Fluid. Mech.*, 2018, **50**, 299–318.
36 A. Giuntoli, F. Puosi, D. Leporini, F. W. Starr and J. F. Douglas, *Sci. Adv.*, 2020, **6**, eaaz0777.
37 Z. Zheng, Y. H. Song, X. Wang and Q. Zheng, *J. Rheol.*, 2015, **59**, 971–993.